Journal of Biomolecular NMR **28:** 213–227, 2004.
KLUWER/ESCOM

Probing slow backbone dynamics in proteins using TROSY-based experiments to detect cross-correlated time-modulation of isotropic chemical shifts

Ananya Majumdar[a] & Ranajeet Ghose[b,c,*]
[a]*Cellular Biochemistry and Biophysics Program, Memorial Sloan-Kettering Cancer Center, New York, NY 10021, U.S.A.;* [b]*Department of Chemistry, City College of the City University of New York, NY 10031, U.S.A.;* [c]*Graduate Center of the City University of New York, NY 10016, U.S.A.*

Received 30 May 2003; Accepted 25 September2003

Key words: cross-correlated relaxation, isotropic chemical shift modulation, multiple-quantum, TROSY

Abstract

The difference in the relaxation rates of zero-quantum (ZQ) and double-quantum (DQ) coherences is the result of three principal mechanisms. These include the cross-correlation between the chemical shift anisotropies of the two participating nuclei, dipolar interactions with remote protons as well as interference effects due to the time-modulation of their isotropic chemical shifts as a consequence of slow μs-ms dynamics. The last effect when present, dominates the others resulting in large differences between the relaxation rates of ZQ and DQ coherences. We present here four sets of TROSY-based (Salzmann et al., 1998) experiments that measure this effect for several pairs of backbone nuclei including ^{15}N, $^{13}C^{\alpha}$ and $^{13}C'$. These experiments allow the detection of the presence of slow dynamic processes in the protein backbone including correlated motion over two and three bonds. Further, we define a new parameter χ which represents the extent of correlated motion on the slow (μs–ms) timescale. This methodology has been applied to ^{15}N,^{13}C,REDPRO-^{2}H-labeled (Shekhtman et al., 2002) human ubiquitin. The ubiquitin backbone is seen to exhibit extensive dynamics on the slow timescale. This is most pronounced in several residues in the N-terminal region of the α-helix and in the loop connecting the strands β_4 and β_5. These residues which include Glu24, Asn25, Glu51 and Asp 52 form a continuous surface. As an additional benefit, the measured rates confirm the dependence of the $^{13}C^{\alpha}$ chemical shift tensor on local secondary structure of the protein backbone.

Introduction

Investigation of the interference effects between two different spin-relaxation mechanisms utilizing the so-called 'cross-correlated' relaxation measurements, has generated a lot of interest in the past several years (Kumar et al., 2000; Frueh, 2002). These studies have complemented standard 'auto-correlated' R_1, R_2 and NOE (Palmer, 2001) measurements by providing detailed information on dynamics including clues into the anisotropy of fast local motion involving several nuclei of the peptide plane (Fischer et al., 1997). In addition to dynamics, these measurements have provided valuable structural information that is very difficult, often impossible, to obtain from conventional measurements. These include the measurement of certain backbone dihedral angles in proteins (Reif et al., 1997; Yang et al., 1997; Chiarparin et al., 1999, 2000; Schwalbe et al., 2001) and sugar puckers in nucleic acids (Richter et al., 1999). Further, they have yielded valuable insight into the nature of the chemical shift tensors for ^{15}N (Fushman et al., 1998), $^{13}C^{\alpha}$ (Tjandra and Bax, 1997) and $^{13}C'$ (Pang and Zuiderweg, 2000) nuclei in solution.

It has been recognized that motions slower than the molecular rotational correlation time, τ_c, includ-

*To whom correspondence should be addressed. E-mail: rghose@sci.ccny.cuny.edu

ing conformational exchange occurring on the μs-ms scale can lead to effects similar to cross-correlated relaxation (Kloiber and Konrat, 2000; Frueh et al., 2001) in multiple-quantum coherences. These slow motions are only capable of modulating the so-called 'isotropic' spin-interactions since the anisotropic interactions are already 'motionally-averaged' by dynamics faster than τ_c. These isotropic interactions include J-couplings and isotropic chemical shifts (Bruschweiler and Ernst, 1992). Unusually large differences in the relaxation rates between zero-quantum (ZQ) and double-quantum (DQ) coherences generated between backbone amide ^{15}N and ^{1}H^{N} (Kloiber and Konrat, 2000) nuclei and those generated between ^{13}C$^{\alpha}$ and sidechain ^{13}C$^{\beta}$ nuclei (Frueh et al., 2001) were explained in terms of the cross-correlated modulation of the isotropic chemical shifts due to slow dynamics. This phenomenon was shown to yield effects similar to those of cross-correlation between the chemical shift anisotropies (CSA) of the two nuclei (*vide infra*) (Kloiber and Konrat, 2000). Chemical shifts may be modulated by conformational dynamics on the μs–ms timescale due to several factors including the formation or disruption of hydrogen bonds, changes in local geometry by alteration of dihedral angles or changes in local chemical environment by repositioning of neighboring aromatic rings. However, a complicating factor is that the modulation, i.e., changes in chemical shift are not uniform for a given set of nuclei affected by the same motion and indeed these may be of either sign and in some cases oppose the effects of the other contributions to the measured relaxation rates. The presence of anisotropic motion may affect the chemical environment of some nuclei and leave others unaffected and blind to the particular motional mode. Thus, as in the case of fast motion, it is necessary to make measurements of multiple relaxation rates involving several nuclei of the protein backbone (Fischer et al., 1997) or sidechain to more accurately characterize the motion. Further, cross-correlated relaxation measurements have the capability to provide information on slow, correlated dynamics over several bonds and thus complement information obtained from CPMG or $R_{1\rho}$ type experiments (Palmer et al., 2001). A clear understanding of correlated motion on all timescales is imperative to allow the interpretation of changes in protein dynamics on complex formation in terms of the energetics of protein-protein interactions (Prompers and Bruschweiler, 2000).

We present here four sets of experiments that measure the difference in the relaxation rates of ZQ and DQ coherences created between pairs of backbone nuclei that include ^{13}C$^{\alpha}$, ^{13}C′ and amide ^{15}N. These experiments are suitable for highly-deuterated proteins and use the TROSY (Salzmann et al., 1998) scheme during magnetization transfer and detection and should be applicable to fairly large proteins. The methodology has been applied to ^{13}C,^{15}N, REDPRO-^{2}H-labeled (Shekhtman et al., 2002) human ubiquitin and demonstrates the existence of slow dynamics on the μs–ms timescale in the protein backbone including correlated motion over several bonds. We define a parameter χ which provides a measure of the extent of this correlated motion. In addition these measurements provide valuable insights into the nature of the ^{13}C$^{\alpha}$ chemical shift tensor in solution.

Materials and methods

Theory

Consider the evolution of the density operator for two spins I and S in a multiple spin system – the difference in relaxation rates between ZQ coherences ($I^+S^- \pm I^-S^+$) and DQ coherences ($I^+S^+ \pm I^-S^-$) leads to the partial conversion $2I_aS_b \rightarrow 2I_{a+\pi/2}S_{b+\pi/2}$ where $(a, b = x, y)$. Thus, if one starts with an initial density operator $\sigma(0) = 2I_aS_b$, in the absence of any extraneous (*vide infra*) relaxation interference effects, coherent chemical shift and scalar coupling evolution, we have, at the end of a relaxation period t_{CC}

$$S_1 = \langle 2I_aS_b(t)\rangle = Ke^{-\Gamma_a t_{cc}} \cosh[\Gamma_{IS}t_{CC}] = \mathrm{Kp}, \tag{1a}$$

$$S_2 = \left\langle 2I_{a+\pi/2}S_{b+\pi/2}(t)\right\rangle = Ke^{-\Gamma_a t_{cc}} \sinh[\Gamma_{IS}t_{CC}] = \mathrm{Kq}, \tag{1b}$$

K is a constant, Γ_a is the auto-correlation rate and $2\Gamma_{IS}$ is the difference in the relaxation rates of the zero-quantum and double-quantum coherences. Thus, if two experiments are performed, one that monitors $\langle 2I_aS_b(t)\rangle$ and another that monitors $\left\langle 2I_{a+\pi/2}S_{b+\pi/2}(t)\right\rangle$, Γ_{IS} is obtained directly from the relationship

$$\frac{S_2}{S_1} = \frac{\left\langle 2I_{a+\pi/2}S_{b+\pi/2}(t)\right\rangle}{\langle 2I_aS_b(t)\rangle} = \tanh(\Gamma_{IS}t_{CC}). \tag{2}$$

The rate Γ_{IS} is given by

$$\begin{aligned}\Gamma_{IS} = & \tfrac{4}{9} B_0^2 \left(\tfrac{2}{5}\tau_C\right) \sum_{i,j=1,2} \left(\sigma_{ii}^I - \sigma_{33}^I\right)\left(\sigma_{jj}^S - \right. \\ & \left.\sigma_{33}^S\right) P_2(Cos\ \theta^{ij}) S_{ij}^2 \\ & + \left(\tfrac{2}{5}\tau_C\right) \sum_k \left(\tfrac{\mu_0 \hbar}{4\pi}\right)^2 \frac{\gamma_H^2 \gamma_I \gamma_S}{r_{IH^k}^3 r_{SH^k}^3} P_2(Cos\theta^k) S_k^2 \\ & + \tfrac{1}{10}\left(\tfrac{2}{5}\tau_C\right)\left(\tfrac{\mu_0 \hbar}{4\pi}\right)^2 \frac{\gamma_I^2 \gamma_S^2}{r_{IS}^6} S_{IS}^2 \\ & + 2\Delta\omega_I \Delta\omega_S p_A p_B \tau_{ex} \\ & = \sum_{i,j} R_{ij}^{CC} + \sum_k R_k^{DD} + R^{XR} + R^{ex}.\end{aligned} \tag{3}$$

The first term in Equation 3 ($\sum_{i,j} R_{ij}^{CC}$) is due to the cross-correlation between the CSA tensors of the two spins I and S. Both tensors have been assumed to be fully asymmetric with components given by σ_{ii}^I and σ_{jj}^S ($\sigma_{11} \leq \sigma_{22} \leq \sigma_{33}$), the projection of the ith component of the CSA tensor of I on the jth component of the CSA tensor of S is given by the angle θ^{ij}; S_{ij}^2 is the Lipari–Szabo order-parameter for the interaction. The second term ($\sum_k R_k^{DD}$) in Equation 3 is due to the cross-correlation between the dipolar interactions of each spin I and S with the proton H^k at a distance r_{IH^k} from spin I and r_{SH^k} from spin S, S_k^2 is the corresponding order parameter and θ^k is the angle subtended by the IH^k and SH^k dipoles. The third term (R^{XR}) is due to the cross-relaxation between I and S nuclei (S_{IS}^2 is the order parameter of the IS internuclear vector). This term is very small ($< 0.07\ s^{-1}$) and is neglected in the present case as are cross-correlation between heteronuclear dipolar interactions. τ_c is the global rotational correlation time (assuming an isotropic overall diffusion tensor) and $P_2(\mathrm{Cos}\theta) = \frac{1}{2}\left(3\mathrm{Cos}^2\theta - 1\right)$. All other terms have their usual meaning. The first three terms of Equation 3 are the result of relaxation in the true sense and depend on the overall correlation time, τ_C whereas the fourth term (R^{ex}) arises due to exchange between two sites A and B with an exchange time τ_{ex}. The populations of the two sites, which we term 'ground' and 'excited' states, are denoted by p_A and p_B respectively. The difference in resonance frequencies between the two states for spins I and S are $\Delta\omega_I$ and $\Delta\omega_S$, respectively (Kloiber and Konrat, 2000). The derivation of Equation 3 is based on the general perturbation framework of Redfield theory and is thus valid for $\tau_c \ll \tau_{\mathrm{ex}} \ll \tau_\sigma$, where τ_σ is an effective chemical shift timescale that is related to $\Delta\omega_I$ and $\Delta\omega_S$. In practice, this puts τ_{ex} in the μs–ms regime.

It is to be remembered that for fast exchange on the chemical shift timescale (i.e. $\tau_{\mathrm{ex}} \ll \tau_\sigma$ is in the μs–ms range) this exchange contribution depends linearly on the exchange time and therefore when present can dominate all other contributions in Equation 3 even when $\Delta\omega_{I,S}$ are small. This linear dependence also occurs in the exchange contributions to single quantum relaxation. However, the excellent sensitivity of multiple quantum relaxation (compared to single quantum relaxation) to exchange arises due to the fact that double-quantum and zero-quantum coherences precess at rates given by the sum ($\omega_I + \omega_S$) and difference ($\omega_I - \omega_S$), respectively, of their resonance frequencies in each state ('ground' and 'excited'). This leads to exchange contributions proportional to $(\Delta\omega_I \pm \Delta\omega_S)^2$ towards zero/double-quantum relaxation rates. Thus depending on the signs of $\Delta\omega_{I,S}$, an enhanced sensitivity to chemical exchange is obtained in either the zero-quantum or double-quantum relaxation even for smaller individual values of $\Delta\omega_{I,S}$. It should also be noted that each of the three major contributions to Equation 3 (excluding the cross-relaxation term) can be of any sign and may interfere with each other.

In deuterated proteins, the first, third and the fourth terms in Equation 3 are unaffected by deuteration. However, each R_k^{DD} in the second term should be replaced by $\left[(1 - f_k) + f_k\,(\gamma_D/\gamma_H)^2\right] R_k^{DD}$ where f_k is the fractional deuteration for the site. It can be shown that this scaling is accurate in the linear regime, i.e., when $\Gamma_{IS} t_{CC} \ll 1$.

Materials and methods

Experimental design

All experiments are derived from HNCA or HN(CO)CA templates. The core element of each sequence is as follows: At an appropriate point, multiple quantum coherence $I_a S_b$ with $(a, b = x, y)$ is generated for the relevant spin pair (I, S = N, C^α or C'), typically, from two-spin order ($I_z S_z$). After a delay t_{CC}, the relevant part of the density operator may be represented as $p\ I_a S_b + q\ I_{a+\pi/\pi 2} S_{b+\pi/2}$, where p and q are coefficients of the 'auto' and 'cross' terms, respectively, as described above in the theory section (Equations 1a,b). Either of these two terms may then be selectively reconverted into two-spin order, depending upon the phases of the subsequent 90° pulses.

These events are summarized below:

$$I_z S_z \xrightarrow{\frac{\pi}{2}(I,S)} I_a S_b (a, b = x, y) \xrightarrow{t_{CC}}$$

$$\left.\begin{array}{l} pI_aS_b \\ + \\ qI_{a+\pi/2}S_{b+\pi/2} \end{array}\right\} \begin{array}{l} \xrightarrow{(\frac{\pi}{2})^{I,S}_{a+\pi/2,b+\pi/2}} \\ \xrightarrow{(\frac{\pi}{2})^{I,S}_{a,b}} \end{array} \begin{array}{l} pI_zS_z \\ qI_zS_z \end{array}.$$

Each experiment is discussed below, utilizing this framework. Unless explicitly stated, in all experiments, the following convention is used: H denotes the amide proton of residue i and N the corresponding amide nitrogen. C′ and C$^\alpha$ correspond to the carbonyl carbon and the alpha carbon of the $(i-1)$th and ith residues respectively.

NC' experiments

This experiment resembles an HNCO sequence, which generates $4H_zN_z^iC_z'^{(i-1)}$ at point A, in Figure 1a. A pair of 90° pulses on C′ and N generates $4H_zN_yC_x'$ multiple quantum coherence. After the t_{CC} delay (point B), the relevant product operators are $4H_zN_yC_x'$ ('auto') and $4H_zN_xC_y'$ ('cross'). Setting the phases of the subsequent 90° (C′,N) pulses to be $\phi_2 = y$, $\phi_3 = x$ or $\phi_2 = x$, $\phi_3 = y$ results in selective reconversion of auto or cross terms, respectively, into $2N_zC_z'$. Two-spin order is then transferred back to the amide nitrogen, which is frequency labeled during the constant-time period T_{NC}. A TROSY (Pervushin, 2000) readout sequence selects the most slowly relaxing component of the N-H spin pair for detection. A brief outline of the magnetization transfer pathway (ignoring signs and trigonometric coefficients) is as follows:

$$H_y \xrightarrow{\tau} H_xN_z \xrightarrow{90_y^H,90_x^N} H_zN_y \xrightarrow{t_{NC'}} H_zN_xC_z' \xrightarrow{90_y^N}$$
$$H_zN_zC_z' \xrightarrow{90_x^N,90_y^{C'}} H_zN_yC_x' \xrightarrow{t_{CC}} (pH_zN_yC_x' +$$
$$qH_zN_xC_y') \xrightarrow{90_{\phi3}^N,90_{\phi4}^{C'}} (p\,or\,q)H_zN_zC_z' \xrightarrow{90_y^N} H_zN_x$$
$$C_z' \xrightarrow{T_{NC},t_1} H^\beta N^\pm(t_1) \xrightarrow{TROSY} H^-N^\beta(t_2),$$

p and q are the coefficients of the auto and cross terms, respectively (see Equations 1a,b), and N^+H^β,$H^-N^\beta$are the slowly relaxing ('TROSY') components of the N–H doublet, in the nitrogen and proton dimensions, respectively.

$NC^{\alpha(i-1)}$ experiments

An HN(CO)CA 'front-end' generates $8H_zN_zC_z^{\alpha(i-1)}C_z'$ at point A, Figure 1b. At this point, the ^{13}C carrier is shifted to the center of the C^α carbons, after which a pair of C^α-selective and ^{15}N 90° pulses generates $8H_zN_yC_x^{\alpha(i-1)}C_z'$ multiple–quantum coherence. During the subsequent t_{CC} period, a C^α selective 180° pulse suppresses evolution under C^α–C' couplings. This pulse can be tailored to avoid exciting most C^β resonances, except Ser and Thr, thus analysis of rates involving the C^α of these residues was not performed. ^{2}H decoupling is maintained throughout the t_{CC} period. At the end of the t_{CC} delay (point B), $8H_zN_yC_x^{\alpha(i-1)}C_z'$ (auto) and $8H_zN_xC_y^{\alpha(i-1)}C_z'$ (cross) terms are generated, both of which are modulated by evolution due to the $J_{NC\alpha^i}$ coupling constant. Although this does not affect the calculation of the cross-correlation rate constant, care is taken to set $t_{CC} < 1/2J_{NC\alpha^i}$. The magnetization transfer pathway until the end of the t_{CC} period is as follows:

$$H_y \xrightarrow{\tau} H_xN_z \xrightarrow{90_y^H,90_x^N} H_zN_y \xrightarrow{t'_{NC}} H_zN_xC_z'$$
$$\xrightarrow{90_y^N,90_x^{C'}} H_zN_zC_y' \xrightarrow{t_{C\alpha C'}} H_zN_zC_z^{\alpha(i-1)}C_x' \xrightarrow{90_y^{C'}}$$
$$H_zN_zC_z^{\alpha(i-1)}C_z' \xrightarrow{90_x^N,90_y^{C\alpha}} H_zN_yC_x^{\alpha(i-1)}$$
$$C_z' \xrightarrow{t_{CC}} (pH_zN_yC_x^{\alpha(i-1)}C_z' + qH_zN_xC_y^{\alpha(i-1)}C_z').$$

A pair of C^α and ^{15}N 90° pulses regenerates $8H_zN_zC_z^{\alpha(i-1)}C_z'$ from the auto or cross term depending upon the phases ϕ_2 ($y \equiv$ auto, $x \equiv$ cross) and ϕ_3 ($x \equiv$ auto, $y \equiv$ cross). The remainder of the sequence is identical to the back end of a TROSY-HN(CO)CA, with ^{15}N frequency labeling during the T_{NC} period in a constant-time fashion followed by a TROSY readout on the amide protons.

$C^{\alpha(i-1)}C'$ experiments

Analogous to the $NC^{\alpha(i-1)}$ sequence, an HN(CO)CA front end generates $8H_zN_zC_z^{\alpha(i-1)}C_z'^{(i-1)}$ at point A, Figure 1c. The ^{13}C carrier is then shifted into the center of the C$^\alpha$ region. A C$^\alpha$ selective 90° pulse, followed immediately by an off-resonance, C′ selective 90° pulse, generates $8H_zN_zC_y^{\alpha(i-1)}C_y'^{(i-1)}$ multiple-quantum coherence. This coherence is refocused at the end of the t_{CC} period by a doubly selective C$^\alpha$/C′ 180° pulse, whose duration is carefully adjusted to minimize phase distortions at both excitation sites. At 14.1 T (600 MHz ^{1}H frequency), for a $\delta_{C^\alpha C'} \approx 18$ kHz, a 1.1 ms Q3 (Emsley and Bodenhausen, 1992) or G3 (Emsley and Bodenhausen, 1990) pulse proved to be sufficient for this purpose. At the end of the t_{CC} period, the coherences $8H_zN_zC_y^{\alpha(i-1)}\ C_y'^{(i-1)}$ (auto) and $8H_zN_zC_x^{\alpha(i-1)}C_x'(i-1)$ (cross) are present. The same set of selective C$^\alpha$/C′ 90° pulses regenerates

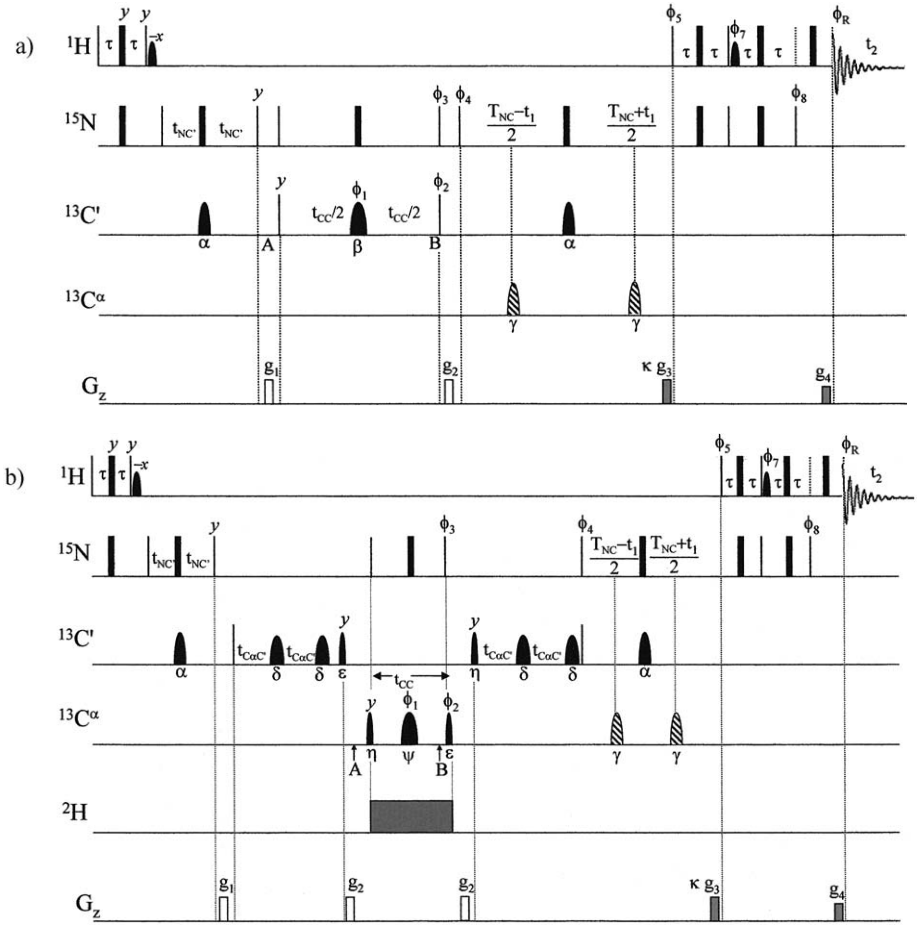

Figure 1. Pulse sequences for measuring cross-correlated modulation of isotropic chemical shifts in multiple quantum coherences involving (a) NC′, (b) NC$^\alpha$, (c) C′ C$^\alpha$ and (d) C$^\alpha$C$^{\alpha(i-1)}$ nuclei. High power 90° and 180° pulses are shown as narrow and wide dark lines, respectively, and 45° pulses by dashed lines. Shaped pulses are shown as sine-bells (thin: 90°, broad: 180°), with on-resonance pulses in black and off-resonance pulses with hatched sine-bells. All pulses were applied with phase x unless explicitly specified. High power pulses were applied with pulse-widths of 5.5 μs (^{1}H), 13.5 μs (^{13}C) and 38 μs (^{15}N). ^{2}H WALTZ16 decoupling during the delay t_{CC} was performed using a 1.0 kHz rf field. RF carriers were placed at 4.75 ppm (^{1}H), 55 ppm (^{13}C$^\alpha$), 175 ppm (^{13}C′), 118 ppm (^{15}N) and 3 ppm (^{2}H). Shaped pulses used were: α: 500 μs G3 (Emsley and Bodenhausen, 1990), for J_{NC^α} or $J_{NC'}$ evolution; β: 1.0 ms Q3 (Emsley and Bodenhausen, 1992), for selective C$^\alpha$/C′ refocusing; δ: 1.5 ms WURST pulses applied in tandem, for adiabatic refocusing and $J_{C'C\alpha}$ evolution (Zweckstetter and Holak, 1998); ε, $\varepsilon^{C'}$: 1.0 ms q-SNEEZE or Q5 (Emsley and Bodenhausen, 1992) pulses for $M_z \rightarrow M_{x/y}$ excitation; $\varepsilon^{C'}$ is phase modulated at 120 ppm for off-resonance excitation at C′. η, $\eta^{C'}$: 1.0 ms time-reversed q-SNEEZE (Kupce and Freeman, 1995) or Q5 pulses for $M_{x/y} \rightarrow M_z$ de-excitation; $\eta^{C'}$ is phase modulated at 120 ppm for off-resonance excitation at C′. γ, $\gamma^{C'}$: 500 μs G3 pulses, phase modulated at −120 and +120 ppm, for off-resonance inversion at C$^\alpha$ and C′, respectively, ψ: 1.1 ms Q3 pulse, phase and amplitude modulated to achieve simultaneous refocusing on-resonance (C$^\alpha$) and at 175 ppm (C′). Relaxation delays (t_{CC} in ms) used were: NC' experiment: 2, 8, 16, 24, 32, 40; NC^α experiment : 2, 8, 12, 16, 20, 24, 28; $C^\alpha C'$ experiment : 2, 8, 16, 24, 32, 40; $C^\alpha C^\alpha$ experiment : 2, 6, 10, 14. τ = 2.75 ms, $t_{NC'}$ = 12 ms, $t_{NC\alpha}$ = 17.0 ms, T_{NC}: 26.0 ms, $t_{C\alpha C'}$: 4.1 ms. Phase cycling: phases ϕ_1, ϕ_2 and ϕ_3 were cycled as follows: (a), (b): $\phi_1 = x,y, \phi_2 = y,y,-y,-y, \phi_3 = 4(x), 4(-x)$; (c): $\phi_1 = x,-x, \phi_2 = x,x,-x,-x, \phi_3 = 4(x), 4(-x)$; (d): $\phi_1 = y,-y, \phi_2 = y, \phi_3 = y,y,-y,-y$; For selection of cross-correlation peaks, phases ϕ_2 and ϕ_3 were simultaneously incremented by 90°. Phases ϕ_4 and ϕ_R (receiver): (a),(b),(c): ϕ_4 = 8(y), 8($-y$), ϕ_R = ABBA, A = ($x,-x,-x,x$), B = ($-x,x,x,-x$); (d): $\phi_4 = 4(y), 4(-y)$, $\phi_R = x,x,-x,-x,-x,-x,x,x$. Phases $\phi_5 = y$, ϕ_7,$\phi_8 = -y$. Gradients: g_1,g_2: 0.5 ms/15 G cm^{-1}; g_3: 1.0 ms, 16 G cm^{-1}; g_4: 0.1 ms, 15.9 G cm^{-1}. Quadrature detection along ω_1 was achieved by inverting the phases ϕ_5, ϕ_7 and ϕ_8, and the sign of the gradient g_3 (κ = ±1) on alternate FIDs and processing the data using the Rance–Kay technique (Rance et al., 1999).

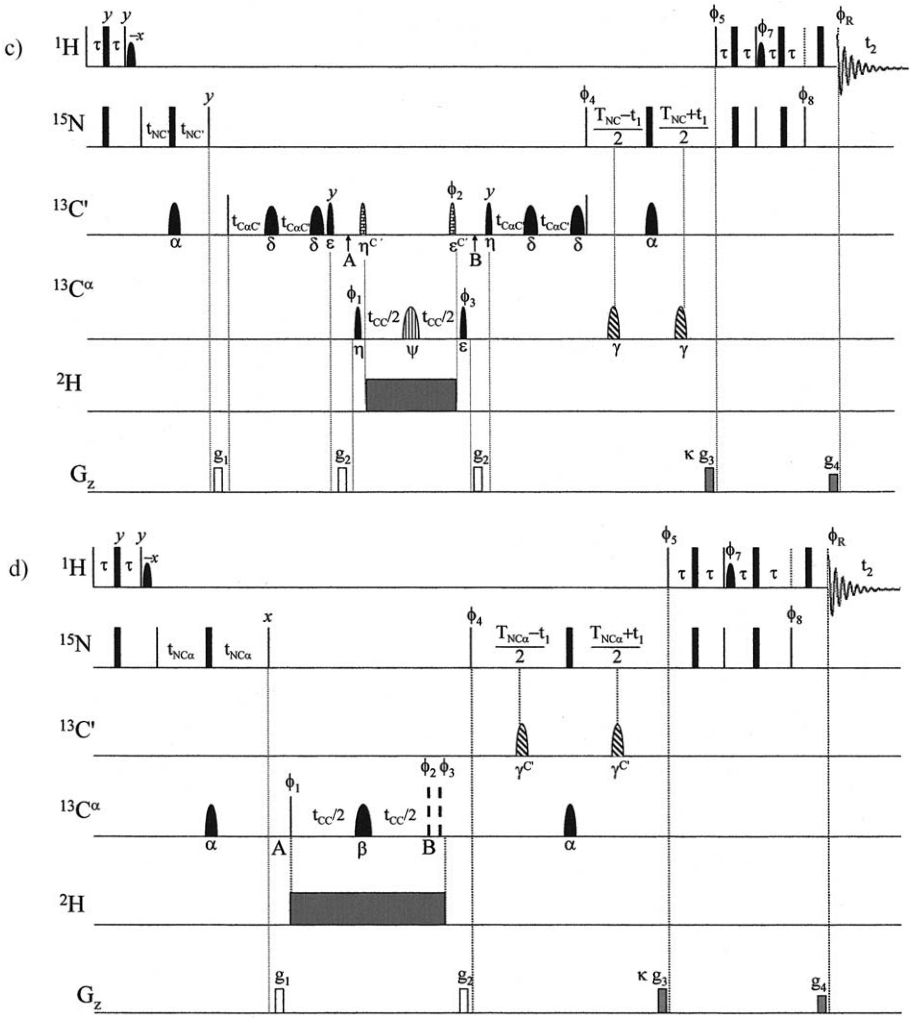

Figure 1. (Continued).

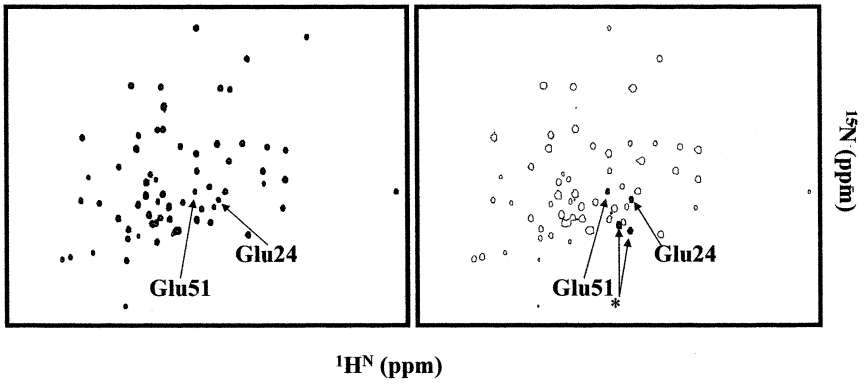

Figure 2. Representative plots of spectra corresponding to 'auto' and 'cross' terms. Shown are plots from the $C'^{(i-1)}C^{\alpha(i-1)}$ experiment (the resonance positions correspond to the ^{15}H,^{1}H^N chemical shifts of the ith residue on which the magnetization is detected). The 'auto' spectrum is shown on the left and the 'cross' spectrum on the right with negative peaks shown with a single contour. The 'auto' spectrum has been phased to be positive. Two residues with significant positive exchange contributions to $\Gamma_{C'C^\alpha}$ are indicated (Glu24 $\Gamma_{C'C^\alpha} = 2.29 \pm 0.67$ s^{-1}, Glu51 $\Gamma_{C'C^\alpha} = 2.83 \pm 0.26$ s^{-1}). The t_{CC} value used was 32.0 ms. Two other strong positive peaks are also seen in the 'cross' spectrum (indicated by *) – these are spurious peaks corresponding to $\Gamma_{C'C^\alpha}$ involving Ser residues (refer to text).

$8H_zN_zC_z^{\alpha(i-1)}C_z^{'(i-1)}$ from the auto or cross term depending upon the phases ϕ_2 and ϕ_3 ($x \equiv$ auto, $y \equiv$ cross). The ^{13}C carrier is then switched back to the C′ region, and coherence transferred to ^{15}N for frequency labeling and subsequent detection on the amide proton, as described above. As before, rates involving Ser or Thr residues were excluded from the analysis. A brief outline is given below:

$$H_y \xrightarrow{\tau} H_xN_z \xrightarrow{90_y^H,90_x^N} H_zN_y \xrightarrow{t_{NC}} H_zN_xC_z' \xrightarrow{90_y^N,90_x^{C'}} H_zN_zC_y' \xrightarrow{t_{C\alpha C'}} H_zN_zC_z^{\alpha(i-1)}C_x' \xrightarrow{90_y^{C'}} H_zN_zC_z^{\alpha(i-1)}C_z' \xrightarrow{90_x^{C'},90_x^{C\alpha}} H_zN_zC_y^{\alpha(i-1)}C_y' \xrightarrow{t_{CC}} (pH_zN_zC_y^{\alpha(i-1)}C_y' + qH_zN_zC_x^{\alpha(i-1)}C_x') \xrightarrow{90_{\phi 2}^{C'},90_{\phi 3}^{C\alpha}} (p\,or\,q)H_zN_zC_z^{\alpha(i-1)}C_z' \xrightarrow{90_y^{C'}} H_zN_zC_z^{\alpha(i-1)}C_x' \xrightarrow{t_{C\alpha C'}} H_zN_zC_y' \xrightarrow{90_y^N,90_x^{C'}} H_zN_xC_z' \xrightarrow{T_{NC},t_1} H^{\beta}N^{\pm}(t_1) \xrightarrow{TROSY} H^-N^{\beta}(t_2).$$

$C^{\alpha}C^{\alpha(i-1)}$ experiments

An HNCA front end generates, at point A, Figure 1d, the following set of coherences: {$2H_zN_y$, $4H_zN_xC_z^{\alpha}$, $4H_zN_xC_z^{\alpha(i-1)}$, $8H_zN_yC_z^{\alpha}C_z^{\alpha(i-1)}$}. A $(90_x^N,90_x^{C^{\alpha}})$ pulse pair creates the desired $8H_zN_zC_x^{\alpha}C_x^{\alpha(i-1)}$ multiple-quantum coherence as well as $2H_zN_z$ two-spin order, while the three-spin operators are dephased by gradients. At the end of the t_{CC} period, the $8H_zN_zC_x^{\alpha}C_x^{\alpha(i-1)}$ term has evolved into $p\,8H_zN_zC_x^{\alpha}C_x^{\alpha(i-1)} + q\,8H_zN_zC_y^{\alpha}C_y^{\alpha(i-1)}$. Nominally, a $(90_x^N,\ 90_{\phi}^{C^{\alpha}})$ pulse pair regenerates $8H_zN_yC_z^{\alpha}C_z^{\alpha(i-1)}$, with the phase $\phi = y$ or x selecting for auto or cross terms, respectively. However, the two-spin order term $2H_zN_z$, is also converted into 'observable' $2H_zN_y$ coherence, which contributes to the detected signal. Alternation of the phase ϕ cannot be used to eliminate this pathway, since the homonuclear $C_a^{\alpha}C_a^{\alpha(i-1)}$ MQ coherence is unaffected by phase alternation ($a = x, y$). In order to eliminate the $2H_zN_y \xrightarrow{90_x^N,90_y^{C^{\alpha}}} 2H_zN_z \xrightarrow{90_x^N,90_{x/y}^{C^{\alpha}}} 2H_zN_y$ pathway, the following approach is used. On one transient, a pair of (45_{ϕ}^C, 45_{ϕ}^C) pulses acts as a composite $90_{\phi}^{C^{\alpha}}$ pulse, which allows both pathways to be detected, with the phase $\phi = y$ or x dictating whether the auto or cross term component of the MQ coherence passes through this filter:

$$\begin{matrix} q8H_zN_yC_z^{\alpha}C_z^{\alpha(i-1)} \\ 2H_zN_y \end{matrix} \xleftarrow{90_x^N} \xleftarrow{45_x^C,45_x^C}$$

$$\begin{bmatrix} p8H_zN_zC_x^{\alpha}C_x^{\alpha(i-1)} \\ q8H_zN_zC_y^{\alpha}C_y^{\alpha(i-1)} \\ 2H_zN_z \end{bmatrix} \xrightarrow{45_y^C,45_y^C} \xrightarrow{90_x^N} p8H_zN_yC_z^{\alpha}C_z^{\alpha(i-1)}. \\ \longrightarrow 2H_zN_y$$

On a second transient, a pair of (45_{ϕ}^C, $45_{-\phi}^C$) acts a net zero degree rotation on the MQ coherences, thereby not allowing them to pass through at all:

$$\begin{bmatrix} p8H_zN_zC_x^{\alpha}C_x^{\alpha(i-1)} \\ q8H_zN_zC_y^{\alpha}C_y^{\alpha(i-1)} \\ 2H_zN_z \end{bmatrix} \xrightarrow{45_{x/y}^C,45_{-x/-y}^C} \xrightarrow{90_x^N}$$

$$\begin{matrix} p8H_zN_yC_x^{\alpha}C_x^{\alpha(i-1)} & \text{invisible} \\ q8H_zN_yC_y^{\alpha}C_y^{\alpha(i-1)} & \text{invisible.} \cdot \\ 2H_zN_y \end{matrix}$$

As a result, only the $2H_zN_y$ coherence is detected. *Subtraction* of the two transients results in the detection of the desirable pure auto or cross-correlation terms. Clearly, one incurs a sensitivity loss owing to the fact that the second transient does not record any useful signal.

In all the experiments described above the 180° pulses applied during the relaxation period t_{CC} eliminate most of the extraneous cross-correlation pathways not considered in Equation 3 and lead to magnetization leakage from the pathway under consideration. Further since we are in the linear regime for all experiments, the build-up of the 'cross' term is independent of all such extraneous relaxation rates (Chiarparin et al., 1999). Also, as stated previously, the C^{α} selective inversion pulses are unable to properly invert C^{α} for Ser and Thr residues. Thus, all rates involving Ser and Thr residues measured by the $NC^{\alpha(i-1)}$, $C^{\alpha(i-1)}C'$ and $C^{\alpha}C^{\alpha(i-1)}$ experiments are excluded from the analyses.

Data processing and analysis

All experiments were performed on a Varian Innova NMR spectrometer operating at 600 MHz and equipped with a triple-resonance HCN probe capable of applying pulsed field gradients along the z-axis. The total number of transients per t_1 point varied from 32 to 256. All experiments (for details see the legend to Figure 1) were performed at 27 °C on a 1.5 mM sample of ^{15}N, ^{13}C and REDPRO-^{2}H-labeled (Shekhtman et al., 2002) human ubiquitin in 30 mM Sodium

Acetate, 10% D_2O and 0.1% NaN_3, pH = 4.6. The data were processed using the NMRPIPE (Delaglio et al., 1995) suite of software. The data was mirrored in the indirect dimension, apodized using a squared cosine-bell function and zero-filled to double the size in both dimensions prior to Fourier transformation. The ratio of the volumes of corresponding peaks from the two complementary experiments $\left(\frac{S_2}{S_1}\right)$ was fit to Equation 2 using in-house software that utilizes the ODRPACK (Boggs et al., 1989) library. Reported errors in Γ_{IS} include both the random (from experimental noise) and model-selection errors and are the 95% confidence bounds estimated from the inverse covariance matrices (1-dimensional for the first three cases and 2-dimensional for the last) of the fits to the experimental data.

Results and discussion

Measurement of $\Gamma_{NC'}$

The rate $\Gamma_{NC'}$ was measured using the pulse sequence shown in Figure 1a. The residues 24, 69 and 73 were too weak in the 'auto' experiments in the present and all successive cases and so were excluded from the analysis. Thus, a total of 69 rates were analyzed. The average value was found to be -1.49 ± 1.05 s^{-1} over the ubiquitin backbone. The minimum and maximum values were -7.65 ± 0.14 s^{-1} and 0.28 ± 0.09 s^{-1} respectively. Representative fits to Equation 2 and the $\Gamma_{NC'}$ values are displayed in Figures 3a and 3b, respectively. The residue on which the magnetization is detected is labeled in Figure 3b. $\Gamma_{NC'}$ has contributions from the cross-correlation between the CSAs of the amide ^{15}N of the ith residue and the carbonyl ^{13}C$'$ of the $(i-1)$th residue, the cross-correlation between the individual dipolar interactions of the ^{15}N(i) and ^{13}C$'(i-1)$ nuclei with the same proton (we neglect dipolar interactions with heteronuclei since these are much smaller in magnitude) and the slow, correlated modulation of the isotropic chemical shifts of the ^{15}N(i) and ^{13}C$'(i-1)$.

The CSA tensor of the amide ^{15}N nucleus has been seen to show some variation both in magnitude and direction over the protein backbone in solution with no clear correlation with local secondary structure (Fushman et al., 1998). The ^{13}C$'$ CSA tensor also shows variations in magnitude and orientation as measured in solution (Pang and Zuiderweg, 2000). The variations in both cases are much larger than those measured in model peptides using solid state NMR (Oas et al., 1987a, b). These variations may come from several sources including the influence of local geometry including hydrogen bonding and indeed of local electrostatic effects that are more complicated in real proteins than in model systems (Sitkoff and Case, 1998). Further, the projection of the two CSA tensors does not have any explicit dihedral angle dependence since it depends only on ω, i.e., on the planarity of the peptide bond. The deviation from planarity of the peptide bond has been shown to be quite small (Hu and Bax, 1997). Assuming overall isotropic tumbling with a correlation time of 4.1 ns, ^{13}C$'$ tensor values from Teng et al., 1992) and $\Delta\sigma_N = -160$ ppm, we estimate a value of -1.27 s^{-1} for the cross-correlation between the CSAs of ^{13}C$'(i-1)$ and ^{15}N (i) nuclei. The contribution due to dipole-dipole cross-correlation also has no explicit dependence on dihedral angles. It however depends on several factors including the proton density about a given site which is related to the level of deuteration around that site and the degree of packing. This effect is dominated by the dipole-dipole cross-correlation with the amide H^N and has been estimated to be -1.46 ± 0.29 s^{-1} in REDPRO-labeled ubiquitin. Thus, very large variations in $\Gamma_{NC'}$ can only be explained by the contribution due to the slow modulation of isotropic chemical shifts. This contribution, as is clear from Equation 3 can be substantially larger than the CSA-CSA and dipole-dipole cross-correlation contributions depending on τ_{ex} and the difference in chemical shifts between the 'ground' and 'excited' states (see Theory section). In order to ascertain which residues were involved in chemical exchange we used the following criterion – those residues that displayed $\Gamma_{NC'}$ values (including both upper and lower confidence bounds for the determined rates) deviating from the mean value by more than twice the standard deviation, were considered to be in exchange. This may be represented mathematically by

$$\delta_{NC'} = \sqrt{\left(\Gamma^i_{NC'} - \left\langle\Gamma^*_{NC'}\right\rangle\right)^2} > 2SD^*_{NC'}. \quad (4)$$

The mean denoted by $\left\langle\Gamma^*_{NC'}\right\rangle$ and standard deviation denoted by $SD^*_{NC'}$ were calculated excluding those residues that satisfy Equation 4. Similar expressions can be written for all the measured rates, namely $\Gamma_{NC'}$, Γ_{NC^α}, $\Gamma_{C'C^\alpha}$ and $\Gamma_{C^\alpha C^\alpha}$ (*vide infra*). This analysis yielded $\left\langle\Gamma^*_{NC'}\right\rangle = -1.35 \pm 0.66$ s^{-1}. Thus using the criterion of Equation 4, it was found that the following pairs of nuclei were undergoing slow correlated dynamics: C$'$(Thr22)-

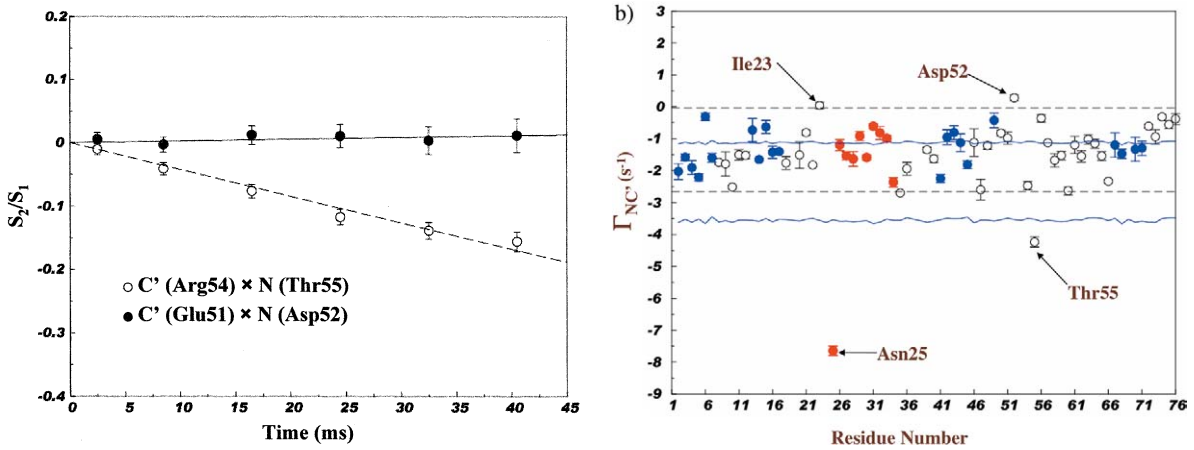

Figure 3. Measurement of $\Gamma_{NC'}$. (a) Representative fits to Equation 2. (b) $\Gamma_{NC'}$ values for ^{15}N,^{13}C,REDPRO-ubiquitin. Residues with significant exchange contributions are labeled. The residue number corresponds to the one contributing the amide ^{15}N to the interacting pair. Sheet, helix and loop residues are represented by blue, red and unfilled circles respectively. The dotted lines indicate twice the standard deviation. The solid blue lines indicate the combined (estimated) contributions of the CSA-CSA and dipole-dipole cross-correlated relaxation. The same representation scheme is used for all subsequent plots of a similar nature. The dipole-dipole contributions to these and all subsequent rates have been calculated using the proton distribution for the REDPRO-labeling scheme using the crystal structure of ubiquitin (1UBQ) (Vijay-Kumar et al., 1987). S^2 values used were 1.0 and 0.6, ^{15}N CSA values used were -125 ppm and -216 ppm (Fushman et al., 1998) for the upper and lower limits, and $^{13}C'$ CSA values and orientations are from Teng et al. (1992).

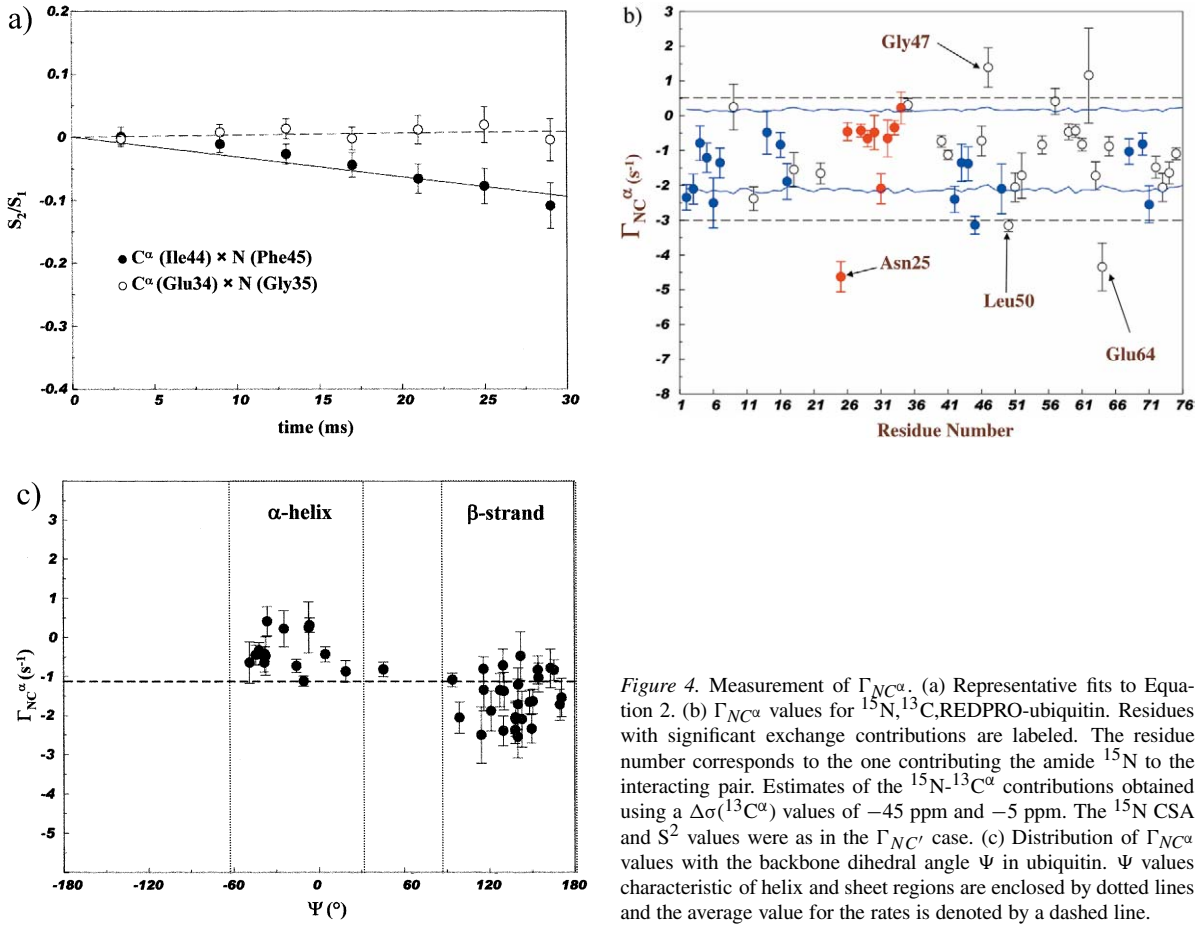

Figure 4. Measurement of Γ_{NC^α}. (a) Representative fits to Equation 2. (b) Γ_{NC^α} values for ^{15}N,^{13}C,REDPRO-ubiquitin. Residues with significant exchange contributions are labeled. The residue number corresponds to the one contributing the amide ^{15}N to the interacting pair. Estimates of the ^{15}N-$^{13}C^\alpha$ contributions obtained using a $\Delta\sigma(^{13}C^\alpha)$ values of -45 ppm and -5 ppm. The ^{15}N CSA and S^2 values were as in the $\Gamma_{NC'}$ case. (c) Distribution of Γ_{NC^α} values with the backbone dihedral angle Ψ in ubiquitin. Ψ values characteristic of helix and sheet regions are enclosed by dotted lines and the average value for the rates is denoted by a dashed line.

N(Ile23), C′(Glu24)-N(Asn25), C′(Glu51)-N(Asp52) and C′(Arg54)-N(Thr55).

Measurement of $\Gamma_{NC^{\alpha(i-1)}}$

Representative fits are shown in Figure 4a and the measured Γ_{NC^α} values are shown in Figure 4b. Due to incomplete inversion of $^{13}C^\alpha$, rates involving Thr or Ser residues were not analyzed (10 residues – 7 Thr, 3 Ser – this was the case in all rates involving $^{13}C^\alpha$ nuclei). The peak volumes for residues 11, 20, 27, 36, 39, 48, 54 and 76, in the 'cross' experiments could not be accurately estimated (errors $> 100\%$ due to signal-to-noise issues) and these were also excluded from the final analysis. Thus a total of 51 rates were analyzed. The rates Γ_{NC^α} (-1.28 ± 1.18 s^{-1}, max $= 1.39 \pm 0.57$ s^{-1}, min $= -4.63 \pm 0.44$ s^{-1}) also have three types of contributions as in the case of $\Gamma_{NC'}$. The dipolar interactions of N(i) and C^α(i$-$1) with remote protons have no explicit dependence on backbone dihedral angles. Using the criterion described in Equation 4, ($\langle\Gamma^*_{NC^\alpha}\rangle = -1.25 \pm 0.88$ s^{-1}), the following pairs of nuclei were shown to display slow, correlated motion over two bonds – C^α(Glu24)-N(Asn25), C^α(Ala46)-N(Gly47), C^α(Gln49)-N(Leu50), C^α(Lys63)-N(Glu64). However, unlike in the case of the amide ^{15}N and carbonyl $^{13}C'$ CSA tensors, the $^{13}C^\alpha$ CSA tensor does have a distinct dependence on the local secondary structure. It has been shown that the differences in CSA values in solution are dominated by changes in tensor orientation between α-helices and β-sheets. In β-sheets, for non-glycine residues, the least shielded component of the $^{13}C^\alpha$ chemical shielding tensor lies almost along the C^α-H^α bond whereas it is roughly orthogonal in helices. The situation is reversed in glycine residues (Havlin et al., 2001). Further, the projection of the ^{15}N and $^{13}C^\alpha$ tensors on each other has an inherent dependence on the backbone dihedral angle Ψ. Thus for the residues without substantial chemical exchange there should be a clear correlation of the rate Γ_{NC^α} with backbone secondary structure and indeed with Ψ. A simple calculation was performed assuming standard α-helix/β-sheet geometries and that the unique component of the amide ^{15}N tensor lies along the NH^N vector and the least shielded component of the $^{13}C^\alpha$ tensor lies along the C^α-H^α bond in sheets and orthogonal to it in helices. The average values for alanine residues from Table 1 of Havlin et al. (2001) for the $^{13}C^\alpha$ shielding tensor components (σ_{ii}), were utilized, other values were as before. We obtained contributions of -1.04 s^{-1} and -0.37 s^{-1} towards Γ_{NC^α} due to $^{13}C^\alpha/^{15}$N CSA-CSA cross-correlation for non-glycine residues in sheets and helices respectively. The contribution of dipole-dipole cross-correlation with the same protons was estimated to be 0.42 ± 0.11 s^{-1} in REDPRO-labeled ubiquitin. Excluding outliers (Equation 4), we find that $\langle\Gamma^*_{NC^\alpha}\rangle_{\text{sheet}} = -1.66 \pm 0.78$ s^{-1} and $\langle\Gamma^*_{NC^\alpha}\rangle_{\text{helix}} = -0.61 \pm 0.66$ s^{-1} showing a clear trend towards smaller absolute values for helices than sheets. Similar trends for the $^{13}C^\alpha$ CSA towards smaller values in helices has been reported previously (Tjandra and Bax, 1998) who obtained a measure of the projection of the $^{13}C^\alpha$ CSA on the $^{13}C^\alpha$-$^1H^\alpha$ internuclear vector. A plot of the measured Γ_{NC^α} values with the backbone dihedral angle Ψ in the crystal structure of ubiquitin (1UBQ) (Vijay-Kumar et al., 1987) is depicted in Figure 4c. Backbone dihedral angles were calculated by the program MOLMOL (Koradi et al., 1996) after adding protons to the crystal structure without any further minimization.

Measurement of $\Gamma_{C'C^\alpha}$

The rate $\Gamma_{C'C^\alpha}$ depends on the cross-correlation between the CSAs of the $^{13}C'(i-1)$ and the $^{13}C^\alpha(i-1)$, on the dipolar couplings of these two nuclei with remote protons and on the correlated modulation of their isotropic chemical shifts due to chemical exchange. In addition to the three weak resonances in the 'auto' experiments and the 10 rates involving Ser or Thr residues, residue 28 was excluded due to a large error ($> 100\%$) in measuring the peak volume in the 'cross' experiment. Thus a total of 58 rates were measured. The average value for the measured rates is -2.78 ± 1.77 s^{-1} with a minimum rate of -6.57 ± 0.85 s^{-1} and a maximum of 2.83 ± 0.26 s^{-1}. The following pair of nuclei were seen to exhibit slow, correlated motions according to the criterion of Equation 4 ($\langle\Gamma^*_{C'C^\alpha}\rangle = -2.98 \pm 1.18$ s^{-1}) $^{13}C^\alpha$(Pro19) – $^{13}C'$(Pro19), $^{13}C^\alpha$(Glu24) – $^{13}C'$(Glu24), $^{13}C^\alpha$(Asn25) – $^{13}C'$(Asn25), $^{13}C^\alpha$(Glu51) – $^{13}C'$(Glu51) and $^{13}C^\alpha$(Asp58)–$^{13}C'$(Asp58). A dependence of $\Gamma_{C'C^\alpha}$ on backbone secondary structure was seen with values of $\langle\Gamma^*_{C'C^\alpha}\rangle_{\text{sheet}} = -2.75 \pm 0.91$ s^{-1} and $\langle\Gamma^*_{C'C^\alpha}\rangle_{\text{helix}} = -3.78 \pm 1.33$ s^{-1} obtained after excluding the outliers. This trend is reflective both of the dependence of the $^{13}C^\alpha$ CSA on secondary structure as well as the projection of the $^{13}C^\alpha$ and $^{13}C'$ CSAs on each other which is expected to be related to the ψ backbone dihedral angle. Estimates of the expected values

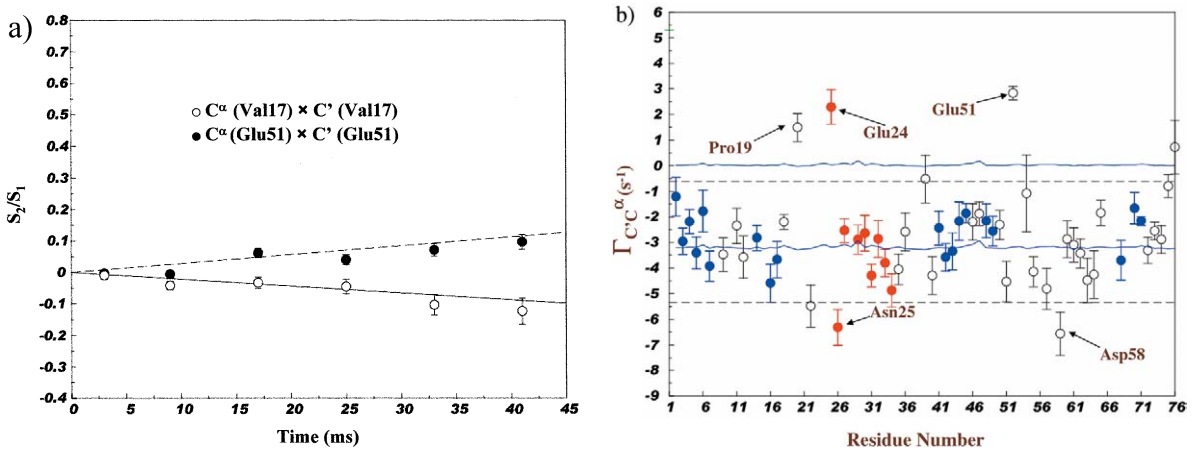

Figure 5. Measurement of $\Gamma_{C'C^\alpha}$. (a) Representative fits to Equation 2. (b) $\Gamma_{C'C^\alpha}$ values for ^{15}N,^{13}C,REDPRO-ubiquitin. Residues with significant exchange contributions are labeled. A value of $\Delta\sigma(^{13}C') = 110$ ppm ($\sigma_{11} - [\sigma_{22} + \sigma_{33}]/2$ from Teng et al.) was used in estimating the CSA-CSA contributions together with $\Delta\sigma(^{13}C^\alpha)$ values of -45 ppm and -5 ppm.

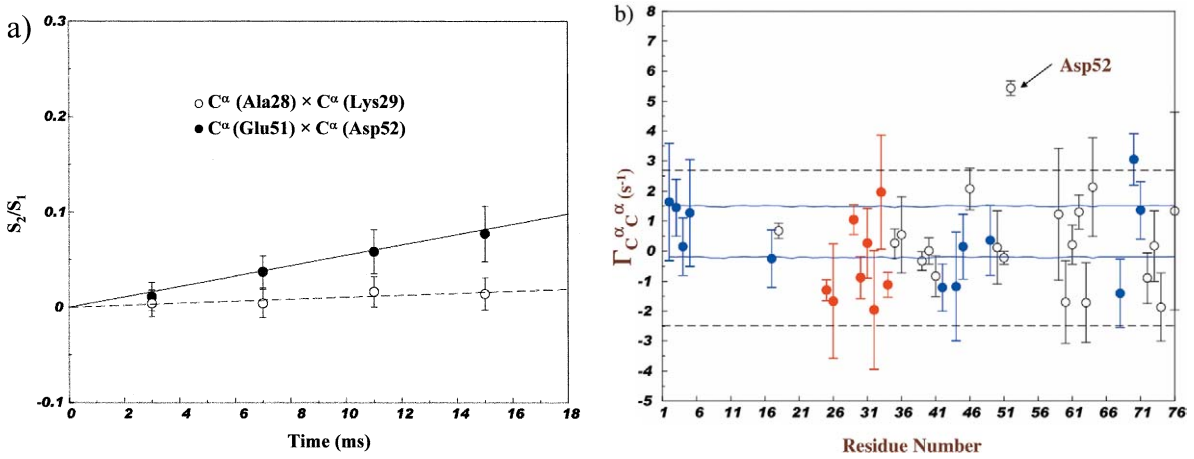

Figure 6. Measurement of $\Gamma_{C^\alpha C^\alpha}$. (a) Representative fits to Equation 2. Fits have been adjusted for the offset. (b) $\Gamma_{C^\alpha C^\alpha}$ values for ^{15}N,^{13}C,REDPRO-ubiquitin. Residues with significant exchange contributions are labeled. The residue number corresponds to that on which the magnetization is detected (see Figure 1d) Estimates of the CSA-CSA contributions were obtained by setting the projection of the two CSAs on each other (i.e., the part within the summation for the first term in Equation 3) to 2500 ppm^2 and -100 ppm^2.

of the CSA-CSA cross-correlation rates in sheets and helices (using ideal helix and sheet geometries and the CSA tensor values described above) were found to be -1.16 s^{-1} and -1.37 s^{-1}, respectively. The dipole-dipole contribution to the rates for REDPRO-labeled ubiquitin was found to be 0.40 ± 0.08 s^{-1}. Representative fits to Equation 2 and the rates for ubiquitin are shown in Figures 5a and 5b, respectively.

Measurement of $\Gamma_{C^\alpha C^\alpha}$

The rate $\Gamma_{C^\alpha C^\alpha}$ provides an excellent indicator of the presence of long-range, correlated motion. The multiple-quantum coherences generated between $^{13}C^\alpha(i-1)$ and $^{13}C^\alpha(i)$ are correlated over three bonds. In this case, the $^{13}C^\alpha$ nuclei for Ser and Thr residues were involved in 20 rates and these were not analyzed due to reasons mentioned previously. Further, the peaks in the 'cross' experiment corresponding to residues 6, 11, 27, 28, 43, 47, 48, 54 and 74 produced large errors in volume measurement and thus were excluded. In the present case, as opposed to the previous three, it was found that inclusion of an offset term in Equation 2 resulted in a statistically significant improvement in the fits. This offset term varied from -0.1% to 0.2%. This is the result of an incom-

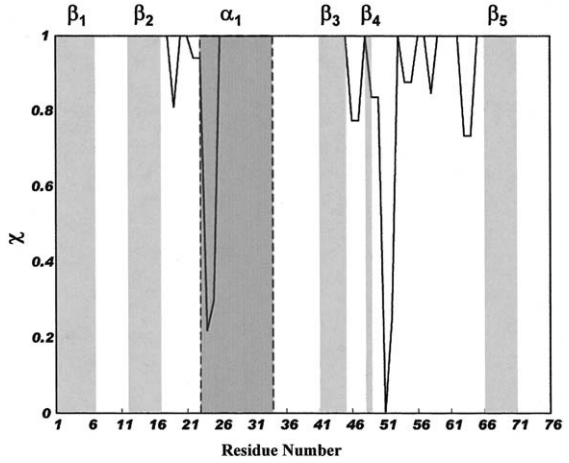

Figure 7. Distribution of χ values in ubiquitin. Values close to 0 indicate extensive slow (μs–ms), correlated motion. Regions with definite secondary structure are indicated. The α-helical region is denoted by the darker shading and enclosed by dotted lines. The β-strand regions are shaded lighter.

plete compensation of the phase errors introduced by the shaped pulses during the relaxation delay, t_{CC}. In all, 40 rates were analyzed and these had an average value of $0.24 \pm 1.53\ s^{-1}$ with a maximum rate of $5.44 \pm 0.24\ s^{-1}$ and a minimum of $-1.96 \pm 1.98\ s^{-1}$. The only pair of nuclei to exhibit correlated motion (according to the classification of Equation 4) over three bonds was $^{13}C^{\alpha}$(Glu51)$-^{13}C^{\alpha}$(Asp52). It was expected that the remaining rates would show a dependence on the dihedral angle Σ (Chiarparin et al., 2000). This angle was shown to be $21° \pm 23°$ in sheets and $-105° \pm 9°$ helices (Chiarparin et al., 2000). This dependence is due to the fact the projection of the CSAs of $^{13}C^{\alpha}$ of successive residues on each other is explicitly dependent on Σ and therefore on secondary structure. A simple calculation using magnitudes and orientation of the $^{13}C^{\alpha}$ CSA tensor as before and assuming that the successive $C^{\alpha}H^{\alpha}$ are antiparallel in β-sheets and orthogonal in α-helices, we obtain the contributions of the cross-correlation between the two CSA tensors towards $\Gamma_{C^{\alpha}C^{\alpha}}$ for sheet regions and helical regions as $0.51\ s^{-1}$ and $0.15\ s^{-1}$. The dipole-dipole contributions were measured to be $-0.14 \pm 0.02\ s^{-1}$ in REDPRO-labeled ubiquitin. The measured rates $\langle \Gamma^{*}_{C^{\alpha}C^{\alpha}} \rangle_{\text{sheet}} = 0.45 \pm 1.36\ s^{-1}$ and $\langle \Gamma^{*}_{C^{\alpha}C^{\alpha}} \rangle_{\text{helix}} = -0.45 \pm 1.40\ s^{-1}$ do reflect this trend of lower predicted rates in helices. Representative fits to Equation 2 and the $\Gamma_{C^{\alpha}C^{\alpha}}$ values in ubiquitin are shown in Figures 6a and 6b respectively.

Comparison of the rates

A comparison of the four measured rates provides more detailed clues into the characteristics of the slow dynamics. We define a factor χ_i for each residue to allow for simple visualization of the regions of the protein which show slow correlated motion as indicated by the four measured cross-correlation rates. χ_i is defined in the following way

$$\chi_i = 1 - \frac{\sum_j \ell_j \delta^i_j}{\text{Max}\left|\sum_j \ell_j \delta^i_j\right|}, \tag{5}$$

ℓ_j is the correlation length for the jth cross-correlation rate corresponding to the number of bonds over which the multiple-quantum coherences are generated. This is 1 for $\Gamma_{NC'}$ and $\Gamma_{C'C^{\alpha}}$; 2 for $\Gamma_{NC^{\alpha}}$ and 3 for $\Gamma_{C^{\alpha}C^{\alpha}}$. $\delta^i_j = f^i_j \sqrt{\left(\Gamma^i_j - \left\langle \Gamma^{*}_j \right\rangle\right)^2}$ with $j = NC'$, $C'C^{\alpha}$, NC^{α}, $C^{\alpha}C^{\alpha}$ and $f^i_j = 1$ if Equation 4 is satisfied and $f^i_j = 0$ otherwise. Thus the χ_i values provide a measure of both the length and degree of correlated motion exhibited by a particular residue and has the value 0 for the residue with the largest degree of slow-correlated motion and 1 for those residues with no motion on this timescale according to the criterion defined by Equation 4 for the four measured cross-correlation rates. It is to be clearly stated here that this approach of denoting the residues with exchange is by no means rigorous and has been used only as a visual representation of the data gleaned from all four experiments. A rigorous approach would involve the measurement of all four terms in Equation 3 and the determination of the Δω values and τ_{ex} values on a per residue basis. The χ values displayed in Figure 7 indicate that extensive motion on the slow timescale is seen at the N-terminus of the α-helix and in several of the loop regions. This kind of motion seems to be very pronounced in the N-terminus of the α-helix and in the loop connecting the fourth and fifth β-stands. A detailed investigation of the individual rates reveals that the nuclei C′(Glu24)$-$C$^{\alpha}$(Glu24)$-$N(Asn25) exhibit correlated motion in the μs-ms timescale as is evident from the large deviations in three of the measured rates, namely $\Gamma_{NC'}$, $\Gamma_{NC^{\alpha}}$ and $\Gamma_{C'C^{\alpha}}$ from their respective mean values. These residues lie in the N-terminal end of the α-helix and Asn25 was shown to undergo extensive conformational exchange from ^{15}N (Tjandra et al., 1995) and ^{13}C relaxation (Lienin et al., 1998) analysis. The relative signs of the

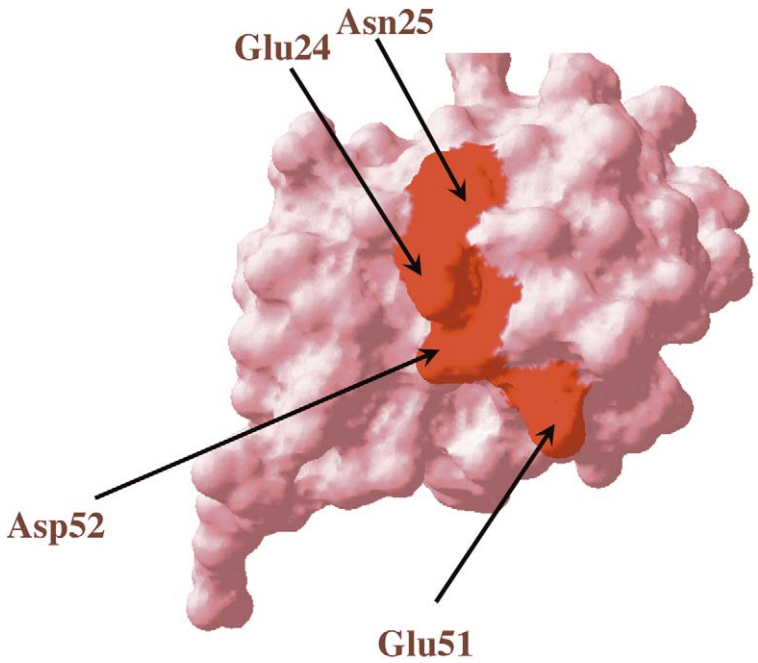

Figure 8. The residues Glu24, Asn25, Glu51 and Asp52 that exhibit the lowest χ values in ubiquitin form a continuous surface (in red).

three measured rates also provide clues into the nature of the changes in the resonance frequencies in the 'ground' and 'excited' states for the three nuclei. $\Gamma_{NC'}$ which involves the C′(Glu24)−N(Asn25) pair has a value which is much lower than the average value. The same behavior is seen for the Γ_{NC^α} involving the C^α (Glu24)−N(Asn25) pair while $\Gamma_{C'C^\alpha}$ involving the C′(Glu24)−C^α(Glu24) pair shows a rate which is much higher than the corresponding mean value. Thus exchange processes make large negative contributions to $\Gamma_{NC'}$ and Γ_{NC^α} and a large positive contribution to $\Gamma_{C'C^\alpha}$. This indicates the $\Delta\omega_{C'}$(Glu24) and $\Delta\omega_C^\alpha$(Glu24) have the same sign with respect to each other and opposite to $\Delta\omega_N$(Asn25) in Equation 3. This implies that the resonance frequency changes between the 'ground' and 'excited' states have the same sense in the three nuclei (γ_N is opposite in sign to γ_C). Another region where extensive long-range correlated motion is seen is in the vicinity of Asp52 which lies in the loop connecting β_4 and β_5. Comparison of the relevant $\Gamma_{NC'}$, $\Gamma_{C'C^\alpha}$ and $\Gamma_{C^\alpha C^\alpha}$ rates reveals correlated motion involving the following : C′(Glu51)−N(Asp52), C^α(Glu51)−C′(Glu51) and C^α(Glu51)−C^α(Asp52), the last of these being correlated over three bonds. These results are consistent with previous studies. Relaxation measurements by Lienin et al. (1998) revealed the existence of a large exchange contribution to the ^{13}C′ R_2 value for Asp52. Neighboring residues have also been shown to be in conformational exchange on the μs–ms timescale in the backbone (Tjandra et al., 1995) (Gly53 resonance is very weak in the HSQC spectrum) and sidechain regions (Leu50) (Frueh et al., 2001). Again, investigation of the individual rates $\Gamma_{NC'}$ (involving the C′(Glu51)−N(Asp52) pair), $\Gamma_{C'C^\alpha}$ (involving the C^α(Glu51)−C′(Glu51) pair) and $\Gamma_{C^\alpha C^\alpha}$ (involving the C^α(Glu51)−C^α(Asp52) pair) reveals that all these values are significantly higher than the corresponding mean values indicating large, positive exchange contributions. Thus comparing the rates we find that $\Delta\omega_{C'}$(Glu51), $\Delta\omega_N$(Asp52), $\Delta\omega_C^\alpha$(Glu51) and $\Delta\omega_C^\alpha$(Asp52) have the same sign with respect to each other. It is interesting that the rate Γ_{NC^α} involving the C^α(Glu51)− N(Asp52) does not show large exchange contributions even though there is correlated motion involving both the C′(Glu51)−N(Asp52), C^α(Glu51)−C′(Glu51) and C^α(Glu51)−C^α(Asp52). A likely explanation is the possibility that $\Delta\omega_{C'}$(Glu51) and $\Delta\omega_C^\alpha$(Glu52) are very large, $\Delta\omega_C^\alpha$(Glu51) has an intermediate value and $\Delta\omega_N$(Asp52) is very small.

A very interesting feature is revealed by mapping the four residues (Glu24, Asn25, Glu51 and Asp52) with very small χ values on the ubiquitin surface.

As is depicted in Figure 8 these four residues form a continuous surface. It is highly probable that the slow dynamics displayed by the two pairs of residues (Glu24-Asn25 and Glu51-Asp52) are correlated with each other and the entire patch comprising these four residues exhibits concerted motion on the slow timescale.

The techniques developed here can be extended to probe the presence of correlated motion in the side-chain regions of proteins. It should thus, in principle, be possible to construct an atom-by-atom view of slow dynamics including correlated motions involving nuclei separated by large distances. This information is not available by present computational strategies. It should be mentioned here that the measured rates also contain information about fast dynamics. After exclusion of the residues that show dynamics and accounting for the variation in the $^{13}C^{\alpha}$ CSA tensor with secondary structure, a clear lack of correlation was seen between the various measured rates in the loop regions and in termini of the sheet and helical regions of ubiquitin. This raises the possibility of variations in CSA tensors (magnitudes of principal components as well as orientation) within a particular secondary structural element (i.e. residue to residue variations along the protein sequence) or to the presence of extensive anisotropic motion on the fast, ps-ns, timescale (Fischer et al., 1997; Pellecchia et al., 1999). Unlike in the case of slow motions, clues on the nature of these fast dynamic modes can be obtained from solvated molecular dynamics (MD) simulations (Fushman et al., 1994; Philippopoulos and Lim, 1995; Philippopoulos et al., 1997; Pfeiffer et al., 2001). A detailed analysis of the effects of fast dynamics on $\Gamma_{NC'}$, $\Gamma_{NC^{\alpha}}$, $\Gamma_{C'C^{\alpha}}$ and $\Gamma_{C^{\alpha}C^{\alpha}}$ is currently under investigation.

Acknowledgements

We thank Dr Alexander Shekhtman for providing the triple-labeled ubiquitin sample. This work has been supported in part by grants from the Research Centers in Minority Institutions (RCMI) initiative of the National Institutes of Health and by the Graduate Research and Teaching Initiative of the State of New York.

References

Boggs, P.T., Donaldson, J.R., Byrd, R.H. and Schnabel, R.B. (1989) *ACM Trans. Math. Software*, **15**, 348–364.

Bruschweiler, R. and Ernst, R.R. (1992) *J. Chem. Phys.*, **96**, 1758–1766.

Chiarparin, E., Pelupessy, P., Ghose, R. and Bodenhausen, G. (1999) *J. Am. Chem. Soc.*, **121**, 6876–6883.

Chiarparin, E., Pelupessy, P., Ghose, R. and Bodenhausen, G. (2000) *J. Am. Chem. Soc.*, **122**, 1758–1761.

Delaglio, F., Grzesiek, S., Vuister, G.W., Zhu, G., Pfeifer, J. and Bax, A. (1995) *J. Biomol. NMR*, **6**, 277–293.

Emsley, L. and Bodenhausen, G. (1990) *Chem. Phys. Lett.*, **165**, 469–476.

Emsley, L. and Bodenhausen, G. (1992) *J. Magn. Reson.*, **97**, 135–48.

Fischer, M.W.F., Zeng, L., Pang, Y., Hu, W., Majumdar, A. and Zuiderweg, E.R.P. (1997) *J. Am. Chem. Soc.*, **119**, 12629–12642.

Frueh, D. (2002) *Prog. Nucl. Magn. Reson. Spect.*, **41**, 305–24.

Frueh, D., Tolman, J.R., Bodenhausen, G. and Zwahlen, C. (2001) *J. Amer. Chem. Soc.*, **123**, 4810–4816.

Fushman, D., Ohlenschlager, O. and Ruterjans, H. (1994) *J. Biomol. Struct. Dyn.*, **11**, 1377–1402.

Fushman, D., Tjandra, N. and Cowburn, D. (1998) *J. Am. Chem. Soc.*, **120**, 10947–10952.

Havlin, R.H., Laws, D.D., Bitter, H.-M.L., Sanders, L.K., Sun, H., Grimley, J.S., Wemmer, D.E., Pines, A. and Oldfield, E. (2001) *J. Am. Chem. Soc.*, **123**, 10362–10369.

Hu, J.-S. and Bax, A. (1997) *J. Am. Chem. Soc.*, **119**, 6360–6368.

Kloiber, K. and Konrat, R. (2000) *J. Biomol. NMR*, **18**, 33–42.

Koradi, R., Billeter, M. and Wüthrich, K. (1996) *J. Mol. Graph.*, **14**, 51–55, 29–32.

Kumar, A., Grace, R.C.R. and Madhu, P.K. (2000) *Prog. Nucl. Magn. Reson. Spect.*, **37**, 191–319.

Kupce, E. and Freeman, R. (1995) *J. Magn. Reson.*, **A112**, 134–37.

Lienin, S.F., Bremi, T., Brutscher, B., Bruschweiler, R. and Ernst, R.R. (1998) *J. Am. Chem. Soc.*, **120**, 9870–9879.

Oas, T.G., Hartzell, C.J., Dahlquist, F.W. and Drobny, G.P. (1987a) *J. Am. Chem. Soc.*, **109**, 5962–5966.

Oas, T.G., Hartzell, C.J., McMahon, T.J., Drobny, G.P. and Dahlquist, F.W. (1987b) *J. Am. Chem. Soc.*, **109**, 5956–5962.

Palmer, 3rd, A.G. (2001) *Annu. Rev. Biophys. Biomolec. Struct.*, **30**, 129–155.

Palmer, 3rd, A.G., Kroenke, C.D. and Loria, J.P. (2001) *Meth. Enzymol.*, **339**, 204–238.

Pang, Y. and Zuiderweg, E.R.P. (2000) *J. Am. Chem. Soc.*, **122**, 4841–4842.

Pellecchia, M., Pang, Y., Wang, L., Kurochkin, A.V., Kumar, A. and Zuiderweg, E.R.P. (1999) *J. Am. Chem. Soc.*, **121**, 9165–9170.

Pervushin, K. (2000) *Q. Rev. Biophys.*, **33**, 161–197.

Pfeiffer, S., Fushman, D. and Cowburn, D. (2001) *J. Am. Chem. Soc.*, **123**, 3021–3036.

Philippopoulos, M. and Lim, C. (1995) *J. Mol. Biol.*, **254**, 771–792.

Philippopoulos, M., Mandel, A.M., Palmer, 3rd, A.G. and Lim, C. (1997) *Proteins*, **28**, 481–493.

Prompers, J.J. and Bruschweiler, R. (2000) *J. Phys. Chem. B*, **104**, 11416–11424.

Rance, M., Loria, J.P. and Palmer, A.G.I. (1999) *J. Magn. Reson.*, **136**, 92–101.

Reif, B., Hennig, M. and Griesinger, C. (1997) *Science*, **276**, 1230–1233.

Richter, C., Griesinger, C., Felli, I., Cole, P.T., Varani, G. and Schwalbe, H. (1999) *J. Biomol. NMR*, **15**, 241–250.

Salzmann, M., Pervushin, K., Wider, G., Senn, H. and Wüthrich, K. (1998) *Proc. Natl. Acad. Sci. USA*, **95**, 13585–13590.

Schwalbe, H., Carlomagno, T., Hennig, M., Junker, J., Reif, B., Richter, C. and Griesinger, C. (2001) *Meth. Enzymol.*, **338**, 35–81.

Shekhtman, A., Ghose, R., Goger, M. and Cowburn, D. (2002) *FEBS Lett.*, **524**, 177–182.
Sitkoff, D. and Case, D. (1998) *Progr. Nucl. Magn. Reson. Spectr.*, **32**, 165–190.
Teng, Q., Iqbal, M. and Cross, T.A. (1992) *J. Am. Chem. Soc.*, **114**, 5312–5321.
Tjandra, N. and Bax, A. (1997) *J. Am. Chem. Soc.*, **119**, 9576–9577.
Tjandra, N. and Bax, A. (1998) *J. Am. Chem. Soc.*, **119**, 9566–9567.
Tjandra, N., Feller, S.E., Pastor, R.W. and Bax, A. (1995) *J. Am. Chem. Soc.*, **117**, 12562–12566.
Vijay-Kumar, S., Bugg, C.E. and Cook, C.J. (1987) *J. Mol. Biol.*, **194**, 531–544.
Yang, D., Konrat, R. and Kay, L.E. (1997) *J. Am. Chem. Soc.*, **119**, 11938–11940.
Zweckstetter, M. and Holak, T.A. (1998) *J. Magn. Reson.*, **133**, 134–147.